Semiconductor Quantum Dots with Environmentally Responsive Mixed Polystyrene/Poly(methyl methacrylate) Brush Layers

Yunyong Guo and Matthew G. Moffitt*

Department of Chemistry, University of Victoria, P.O. Box 3065, Victoria, BC V8W 3V6, Canada

Received April 11, 2007; Revised Manuscript Received June 1, 2007

ABSTRACT: The synthesis and characterization of semiconductor quantum dots (QDs) with mixed polystyrene/poly(methyl methacrylate) (PS/PMMA) polymer brush stabilizing layers are described. Synthesis involves micellization of a PS-*b*-PAA-*b*-PMMA triblock copolymer, followed by growth of cadmium sulfide (CdS) QDs in the ionic cores. These environmentally responsive hybrid nanoparticles are studied in various solvents with different polarities (acetone, THF, chloroform, and toluene). Static and dynamic light scattering results indicate conformational changes in the mixed brush structure in response to different solvent polarities which allow the "smart" nanoparticles to maintain colloidal stability; UV−vis and photoluminescence spectra demonstrate that QD sizes and optical properties are independent of the solvent medium due to protection by the block copolymer. Long-term stability of QD size distributions in most investigated solvents is demonstrated for periods of up to 6 months. 2D ^{1}H NOESY experiments indicate that PS and PMMA chains are statistically distributed around the QDs within the mixed brush layer. It is also shown that the mixed brush QDs can be dispersed in both PS and PMMA homopolymers due to their environmentally responsive mixed brush layers.

Introduction

Colloidal metal and semiconductor nanoparticles have received widespread attention due to their immense potential for applications ranging from biological labeling and diagnostics to photonics and all-optical computing. In recent years, it has been recognized that the utilization of nanoparticles as building blocks within various devices will require their controlled assembly into one-, two-, and three-dimensional superstructures organized on multiple functional length scales. As well, the incorporation of colloidal nanoparticles into polymer environments offers the added advantage of combining the properties of nanoparticles with the mechanical, optical, and electronic properties of specific polymers. Hybrid building blocks consisting of an inorganic nanoparticle core and an external stabilizing polymer brush layer provide a range of interesting routes toward dispersion or controlled self-assembly of nanoparticles within polymers. A wide range of strategies have been employed to generate polymer brush-stabilized nanoparticles, including polymerizations from the surface of colloidal nanoparticles,[1−6] specific binding or ligand exchange with functionalized polymers,[7−14] and growth or encapsulation of nanoparticles within block copolymer micelles.[15−28]

In the above examples, the polymer brushes surrounding the nanoparticles consist of a single type of polymer chain which responds uniformly to an external stimulus such as changes in temperature or the surrounding solvent. A key challenge in the self-assembly of such "dumb" particles into interesting superstructures is their inherent lack of anisotropic interparticle interactions, resulting in a thermodynamic tendency either to be uniformly dispersed in the surrounding medium or to undergo macroscopic phase separation. In our group, we extensively studied cadmium sulfide (CdS) quantum dots (QDs) encapsulated within diblock copolymer micelles which contribute an external homogeneous polystyrene (PS) brush layer;[20,29] such particles (termed PS−CdS) can be "tricked" into forming mesoscale spheres in aqueous media,[30,31] or mesoscale wires and cables at the air−water interface,[32,33] by blending with amphiphilic block copolymers which regulate their self-assembly. We have also shown that phase separation between PS−CdS and PMMA homopolymer within spin-coated polymer blend films gives rise to various hierarchical QD/polymer patterns at the micron scale, including networks of wires and arrays of spatially correlated islands.[34] Although reproducible, these various superstructures form under nonequilibrium conditions, currently limiting the complexity of nanoparticle self-assembly within polymers.

For many applications, the quest for reversible thermodynamic self-assembly of nanoparticles into a variety of complex 3D superstructures has created a need for more sophisticated hybrid building blocks.[35−38] Very recently, several examples of colloidal nanoparticles coated with mixed brushes of two different types of homopolymers have appeared in the literature.[39−44] Such hybrid particles can be regarded as "smart" particles, since external stimuli such as solvent or temperature changes result in conformational reorganization of the mixed brush, which can dramatically change the surface properties of the polymer layer. Li et al. carried out ATRP from Y-initiator-modified silica nanoparticles to produce mixed poly(*tert*-butyl acrylate)/polystyrene (PtBA/PS) brushes.[39] Subsequent hydrolysis resulted in amphiphilic nanoparticles with a mixed poly(acrylic acid)/polystyrene (PAA/PS) layer which were soluble in both chloroform (a good solvent for PS chains) and water (a good solvent for PAA chains). Shan et al. used a "grafting-to" approach to produce mixed brush amphiphilic gold nanoparticles by reducing $HAuCl_4 \cdot xH_2O$ in the presence of a mixture of dithioester-terminated poly(*N*-isopropylacrylamide) (PNIPAM) and PS chains.[40,41] When these particles were cast at the air−water interface from a spreading solvent, the mixed brushes reorganized with PNIPAM chains spreading on the water surface and PS chains collapsing into globules.[41] Using a similar "grafting-to" approach, Chiu et al. synthesized gold nanoparticles coated with mixed brushes of poly(2-vinylpyridine) (PVP) and PS chains, which were found to localize at the interface of PS and PVP domains when blended with a PS-*b*-PVP block copolymer.[42] Zubarev and co-workers used a surface polymerization strategy to form amphiphilic gold nanoparticles with

10.1021/ma070855x CCC: $37.00
Published on Web 07/03/2007

Scheme 1. Formation of PS/PMMA−CdS via Self-Assembly of PS-*b*-PAA-*b*-PMMA Triblock Copolymers, Followed by Templated QD Growth in the Copolymer Micelle Cores

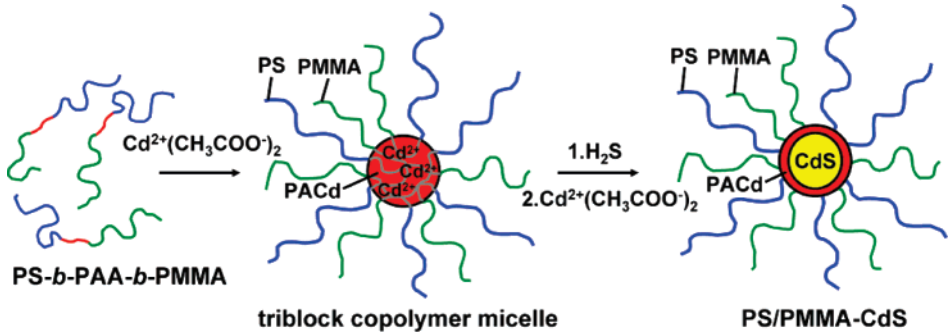

V-shaped ligands consisting of either polybutadiene−poly(ethylene oxide) (PB−PEO) or polystyrene−poly(ethylene oxide) (PS−PEO) arms.[43] Interestingly, they showed that the mixed brush PS−PEO nanoparticles underwent a conformational rearrangement during water addition to THF solutions, forming nanoparticle amphiphiles with linear symmetry that self-assembled into 1D wormlike superstructures.[44]

A different route to nanoparticles with mixed polymer brushes involves the self-assembly of triblock copolymers with an insoluble core-forming center block and two different soluble end blocks.[45−48] Erdhardt et al. employed bulk microphase separation of a polystyrene-*block*-polybutadiene-*block*-poly(methyl methacrylate) (PS-*b*-PB-*b*-PMMA) triblock copolymer with a relatively short center block to generate a morphology of PB nanospheres distributed at the interface of a PS/PMMA lamellar structure.[45] Chemical cross-linking of the PB spheres resulted in "Janus" PS/PMMA mixed brush micelles which could be dispersed in various organic solvents[45] and underwent self-assembly into surface aggregates at the air−water interface.[46] Subsequent hydrolysis of the PMMA chains resulted in amphiphilic spheres which formed supermicelles in aqueous media.[47] Liu and co-workers have formed amphiphilic micelles with mixed coronal chains via self-assembly of a poly(butyl methacrylate)-*block*-poly(2-cinnamoyloxyethyl methacrylate)-*block*-poly(*tert*-butyl acrylate) (PBMA-*b*-PCEMA-*b*-P*t*BA) triblock copolymer, followed by cross-linking of the PCEMA cores and hydrolysis of PtBA coronal chains.[48] These examples demonstrate that triblock copolymer self-assembly is an interesting route toward environmentally responsive nanoparticles with a mixed brush external layer. However, in the triblock copolymer systems explored to date, the mixed-brush nanoparticles possess cores comprised solely of cross-linked polymers without interesting optical properties.

The present work utilizes self-assembly of a triblock copolymer to synthesize the first example of semiconductor QDs possessing environmentally responsive mixed polymer brush layers (Scheme 1). First, the micellization of a polystyrene-*block*-poly(acrylic acid)-*block*-poly(methyl methacrylate) (PS-*b*-PAA-*b*-PMMA) triblock copolymer in organic solvent is induced by cadmium acetate addition and ionization of the relatively short PAA blocks; self-assembly forms poly(cadmium acrylate) (PACd) ionic cores surrounded by mixed coronae of PS and PMMA chains. Next, the micelle cores are reacted with hydrogen sulfide (H_2S), resulting in growth of CdS QDs with a mixed polymer brush layer (PS/PMMA−CdS). We show that these particles can be dispersed in solvents of wide-ranging polarities while maintaining both colloidal stability and stability of QD optical properties. Structural characterization of PS/PMMA−CdS particles by 2D ^{1}H NOESY NMR and static and dynamic light scattering indicates conformational changes in the mixed brush in response to different solvent environments. We also show that PS/PMMA−CdS QDs can be uniformly dispersed in both PS and PMMA homopolymers via spin-coating. These semiconductor QDs coated with mixed polymer brushes represent an important step toward a new type of "smart" self-assembling element for nanostructured polymer/QD materials and devices.

Experimental Section

Synthesis of Polystyrene-*b*-poly(*tert*-butyl acrylate)-*b*-poly(methyl methacrylate) (PS-*b*-P*t*BA-*b*-PMMA) Triblock Copolymer. The triblock copolymer used as a precursor material in the present study was synthesized using anionic polymerization techniques described elsewhere in the literature.[49,50] All monomers were stirred over calcium hydride for 24 h, distilled under vacuum, and stored under nitrogen at −20 °C. Immediately prior to the polymerization reaction, styrene, *tert*-butyl acrylate, and methyl methacrylate monomers (Aldrich) were further purified by the addition of fluorenyllithium to styrene, and triethylaluminum to *tert*-butyl acrylate and methyl methacrylate, followed by vacuum distillation into flame-dried cylinders. The tetrahydrofuran (THF) reaction solvent was freshly distilled following reflux over sodium/benzophenone. Solvents, monomers, and initiator were transferred using rigorous Schlenk-line techniques under ultrahigh-purity (UHP) nitrogen atmosphere and vacuum.

Several drops of α-methylstyrene (Aldrich) were added to the reaction flask containing LiCl (10 mol of LiCl:1 mol of *sec*-butyllithium) dissolved in THF. The *sec*-butyllithium initiator (1.3 M in hexanes, Aldrich) was then added dropwise until a dark red color persisted, followed by the addition of the desired quantity of initiator. The reaction flask was cooled to −78 °C using a dry ice/acetone bath, followed by the sequential addition of styrene, *tert*-butyl acrylate, and methyl methacrylate monomers, allowing 30 min for the polymerization of each block. Aliquots of the reaction mixture were withdrawn following polymerization of each of the first two blocks (PS and P*t*BA) for analysis by gel permeation chromatography (GPC). Finally, the polymerization reaction was terminated by the addition of degassed methanol.

Selective Hydrolysis of PS-*b*-P*t*BA-*b*-PMMA. The P*t*BA block of PS-*b*-PtBA-*b*-PMMA was selectively hydrolyzed to form polystyrene-*b*-poly(acrylic acid)-*b*-poly(methyl methacrylate) (PS-*b*-PAA-*b*-PMMA) by reflux in toluene with *p*-toluenesulfonic acid (5 mol % relative to the *tert*-butyl acrylate content) for 5 h. ^{1}H NMR was used to confirm that the PtBA block was completely hydrolyzed without significant hydrolysis of the PMMA block.

Preparation of Polystyrene-*b*-poly(cadmium acrylate)-*b*-poly(methyl methacrylate) (PS-*b*-PACd-*b*-PMMA) Micelles. The methodology used for preparing PS-*b*-PAA-*b*-PMMA triblock copolymer-stabilized QDs was similar to that described previously for forming PS-*b*-PAA diblock copolymer-stabilized QDs.[17,20] The triblock copolymer was dissolved in benzene/methanol (90:10 v/v) at a concentration of ca. 2 wt %. The formation of reverse micelles via self-assembly of insoluble PACd cores was induced by the addition of excess 0.25 M cadmium acetate dihydrate (Aldrich) in

methanol (1.5 mol of cadmium acetate dihydrate:1 mol of acrylic acid repeat units) followed by stirring of the solution for 4 h. The onset of a bluish tinge to the solution with cadmium acetate addition suggested an increase in light scattering caused by the formation of micelles. The material was recovered by freeze-drying and then dried in a vacuum oven at 70 °C for 24 h. Excess cadmium acetate was removed by washing the freeze-dried powder repeatedly with methanol followed by drying under vacuum at 70 °C for 24 h.

Preparation of Mixed Polymer Brush-Stabilized QDs (PS/PMMA−CdS). The white powder consisting of freeze-dried PS-*b*-PACd-*b*-PMMA micelles (PACd cores and mixed PS/PMMA coronae) was exposed to an atmosphere of 100% humidity for a period of 1 week. The powder was then exposed to wet H_2S for 9 h, resulting in CdS QD formation in the PACd cores, and then stored under active vacuum for 12 h to remove excess H_2S. To stabilize the resulting micelle-encapsulated QDs, the yellow powder was dispersed in THF (2 wt %), and excess cadmium acetate dihydrate in methanol (2 mol of cadmium acetate dihydrate:1 mol of acrylic acid repeat units) was added to reneutralize the acrylic acid blocks. After overnight stirring, the sample was recovered by precipitation into methanol, then washed repeatedly with methanol, and dried for 24 h in a vacuum oven at 70 °C. This final product was designated PS/PMMA−CdS.

Dispersion of PS/PMMA−CdS in PS or PMMA Homopolymers. Films were prepared by solution-blending PS/PMMA−CdS QDs with either PS homopolymer (prepared in our lab by anionic polymerization: $M_n = 130\,000$ g mol^{-1}, $M_w/M_n = 1.01$) or PMMA homopolymer (Aldrich, $M_w = 120\,000$ g mol^{-1}). All blend components were first dissolved separately in toluene to 6 wt % polymer and allowed to stir overnight. Two different blends were then prepared by mixing component solutions in appropriate ratios: (1) PS/PMMA−CdS/PS and (2) PS/PMMA−CdS/PMMA, each with PS/PMMA−CdS:homopolymer ratios of 30:70 (w/w). The solutions were stirred for 2 h then left overnight to equilibrate. Blend films were prepared by spin-coating blend solutions onto clean glass microscope coverslips at a spinning rate of 3000 rpm. All films were dried overnight under vacuum at 70 °C before analysis.

Gel Permeation Chromatography (GPC). GPC measurements were performed using a Viscotek model 302 liquid chromatography system equipped with refractive index (RI), low-angle light scattering (LALS, $\theta = 7°$), right-angle light scattering (RALS, $\theta = 90°$), and UV detectors. THF was used as the eluent at a flow rate of 1 mL/min, and the column temperature was set at 35 °C. All polymer solutions were filtered through membrane filters with a nominal pore size of 0.45 μm before injection into the GPC column. The data were collected and analyzed on a Dell Dimension 2300 computer with appropriate GPC software from Viscotek. Two ViscoGEL HR high-resolution columns (styrene−divinylbenzene columns) in series were used: G3000 HR 60 k and GMHHR-M Mixed Bed 4 M columns. The molecule weight distribution for the PS block of the triblock copolymer was determined from GPC data using an algorithm from Viscotek, which relies on LALS detection from a 670 nm diode laser source.

^{1}H NMR Analysis. ^{1}H NMR spectra of triblock copolymers and micelles were recorded using a Bruker AC 300 MHz spectrometer. 2D ^{1}H nuclear Overhauser effect spectroscopy (NOESY) experiments were made at 300 K on a Bruker Avance 500 MHz spectrometer. For the 2D NOESY spectra, 256 experiments of 2000 data points were recorded, consisting of 8 scans per increment, using standard Bruker software. The clearest contour plots were obtained using a mixing time of 300 ms.

UV−vis Absorption and Photoluminescence Measurements. Absorption spectra were recorded on a Cary 50-scan UV−vis spectrophotometer. Static photoluminescence (PL) measurements were recorded on an Edinburgh Instruments FLS 920 instrument equipped with a Xe 450 W arc lamp and a red-sensitive PMT (R928-P). Typical PL measurements involved $\lambda_{ex} = 400$ nm excitation and collection of emitted light with a long-pass 450 nm emission filter in place. For PL measurements of QDs in solution, the PS/PMMA−CdS sample was dispersed in various solvents (spectroscopic grade acetone, chloroform, THF, and toluene) at concentrations such that the measured absorbance at 400 nm was less than 0.1. For PL measurements of polymer blend films on glass, front-face excitation of the films was used, with an angle of ca. 45° between the detector and the film normal. All spectra were collected at 1 nm spectral resolution, and the appropriate background was subtracted.

Static and Dynamic Light Scattering Measurements. Static light scattering (SLS) and dynamic light scattering (DLS) experiments were carried out on a Brookhaven Instruments photon correlation spectrometer equipped with a BI-200SM goniometer, a BI-9000AT digital autocorrelator, and a Melles Griot He−Ne Laser (632.8 nm) with a maximum power output of 75 mW. To ensure the accuracy for both SLS and DLS measurements, great care was taken to eliminate dust from the samples. Spectroscopic grade acetone, chloroform, THF, and toluene were filtered through two membrane filters with 0.20 μm nominal pore size connected in series. Stock solutions (ca. 5 mg/mL) of PS/PMMA−CdS colloids in various solvents were prepared the night before SLS or DLS measurements to ensure equilibration and then filtered through two membrane filters with 0.45 μm nominal pore size connected in series to remove dust. All scintillation vials were thoroughly cleaned with filtered solvent before stock solutions of the PS/PMMA−CdS colloids were transferred into the vials. Successive dilutions of the colloids were carried out by adding known quantities of the filtered solvents.

SLS measurements of PS/PMMA−CdS in various solvents were carried out in a concentration range from 0.2 to 1 mg/mL. For each concentration, angles of detection from 15° to 155° were measured with 15° increments between angles. Ten repeat measurements of scattered light intensity were taken at each angle and concentration to obtain Zimm plots based on the fundamental Zimm equation for light scattering from polymer solutions:

$$\frac{Kc}{\Delta R_\theta} = \frac{1}{M_w P(\theta)} + 2A_2 c \qquad (1)$$

where ΔR_θ is the excess Rayleigh scattering ratio, $P(\theta)$ is the particle scattering factor, M_w is the apparent weight-average molecular weight of the sample, A_2 is the second virial coefficient, c is the polymer concentration, and K is a composite of optical and fundamental constants. For each solvent, reported values of M_w and root-mean-square z-average radii of gyration, r_g, were determined from the average results of three separate Zimm plots obtained from different stock solutions; average errors on M_w and r_g values were 7%. All SLS measurements were conducted at 23 °C.

The differential refractive index values, dn/dc, for PS/PMMA−CdS dispersed in acetone, chloroform, THF, and toluene were required for Zimm plot analysis of static light scattering results. These were determined using a BI-DNDC differential refractometer which was calibrated using a known standard of potassium chloride (KCl) in water. Stock solutions of PS/PMMA−CdS of ca. 10 mg/mL were diluted to obtain five concentrations from 1 to 5 mg/mL for dn/dc determination. Three repeat measurements of dn/dc were obtained for PS/PMMA−CdS in each solvent.

DLS measurements of PS/PMMA−CdS in each solvent were conducted at five different angles, 35°, 50°, 70°, 90°, and 120°, and at various concentrations in the range 0.02−1 mg mL^{-1}. For each angle and concentration, three repeat measurements of the autocorrelation function were obtained. Average errors on hydrodynamic radii, r_h, determined for each solvent from DLS at multiple angles and several concentrations were 4%. All DLS measurements were conducted at 23 °C.

Laser Scanning Confocal Fluorescence Microscopy (LSCFM). Laser scanning confocal fluorescence microscopy measurements of polymer blend films containing PS/PMMA−CdS were done on a Zeiss LSM 410 equipped with an Ar/Kr laser. A Zeiss Plane-Aprochromat 63× oil immersion objective was used. All films were excited at ~488 nm, using a band-pass 485 ± 20 nm line selection filter and a FT 510 dichroic beam splitter. A long-pass 515 nm

emission filter was used such that only light above 515 nm reached the PMT. A pinhole diameter of 0.984 Airy units was used for all measurements, resulting in an optical section thickness of 0.62 μm fwhm.

Transmission Electron Microscopy. TEM was performed on a Hitachi H-700 electron microscope, operating at an electron accelerating voltage of 75 kV. Solution-cast samples were prepared by depositing a drop of 2 mg/mL PS/PMMA−CdS solution in benzene on a copper grid (300 mesh) coated with an amorphous carbon film and immediately blotting excess solution; the grids were then dried at room temperature for 2 h before imaging. For TEM of polymer blends of PS/PMMA−CdS dispersed in PS or PMMA homopolymer, the films were first were first embedded in an Epon resin, and then ~50 nm thick sections were produced with a diamond knife on Reichert UltraCut E ultra-microtone. The thin sections were placed on carbon/Formvar-coated 300 mesh copper grids for imaging.

Results and Discussion

Characterization of PS-*b*-P*t*BA-*b*-PMMA and Hydrolyzed PS-*b*-PAA-*b*-PMMA Triblock Copolymers. During anionic polymerization of the triblock copolymer, progressive growth of living chains after the addition of each monomer component was followed by GPC (Supporting Information). Following styrene polymerization, GPC revealed a single narrow peak with number-average molecular weight $M_n = 30\,800$ g mol^{-1}, from which the number-average degree of polymerization of the PS block was determined ($N_{PS} = 296$). Subsequent polymerization of *tert*-butyl acrylate and methyl methacrylate resulted in the single GPC peak progressively shifting to lower elution volumes, indicating growth of the living chain to form a P*t*BA middle block and PMMA end block. GPC of the PS-*b*-P*t*BA-*b*-PMMA triblock copolymer after termination of the living chains revealed a very narrow polydispersity with $M_w/M_n = 1.05$.

The ^{1}H NMR spectrum of the synthesized copolymer confirmed incorporation of PS, P*t*BA, and PMMA blocks and allowed the relative block lengths to be determined via integrated intensities of characteristic resonances. The spectrum and key proton peak assignments are shown in Figure 1. Most important for composition determination were resonances at $\delta = 7.07$ ppm and $\delta = 6.57$ ppm (5 phenyl ring protons from each styrene repeat unit), $\delta = 3.59$ ppm (3 methyl ester protons from each methyl methacrylate repeat unit), and $\delta = 1.42$ ppm (an overlap of 2 methylene protons from each styrene repeat unit and 9 *tert*-butyl ester protons from each *tert*-butyl acrylate repeat unit).[51] Based on the relative integrated intensities of these resonances, the mole fractions of PS, P*t*BA, and PMMA repeat units in the copolymer could be determined: $x_{PS} = 0.52$, $x_{PtBA} = 0.07$, and $x_{PMMA} = 0.41$. From these mole fraction values, and the number-average degree of polymerization of the PS block determined by GPC ($N_{PS} = 296$), the number-average degrees of polymerization of the PtBA and PMMA blocks were assigned: $N_{PtBA} = 41$ and $N_{PMMA} = 236$. The characterized triblock copolymer before selective hydrolysis was therefore designated PS(296)-*b*-P*t*BA(41)-*b*-PMMA(236), with numbers in parentheses representing the number-average degrees of polymerization of the respective blocks.

The ^{1}H NMR spectrum of the copolymer following the hydrolysis reaction confirmed that the central P*t*BA block had been selectively hydrolyzed to PAA, without significant hydrolysis of the PMMA block. The spectrum and key proton peak assignments following hydrolysis are shown in Figure 2. Compared to the spectrum obtained before hydrolysis, the intensity of the $\delta = 1.42$ ppm resonance has decreased considerably: after hydrolysis, the integrated intensity ratio of the $\delta = 1.42$ ppm peak to the phenyl ring protons ($\delta = 7.07$ ppm and $\delta = 6.57$ ppm) was determined to be 0.40, which is the predicted ratio of methylene to phenyl ring protons on styrene (2/5), confirming that the overlapping *tert*-butyl ester resonance at $\delta = 1.42$ ppm has completely disappeared. As well, the integrated ratio of the phenyl ring protons ($\delta = 7.07$ ppm and $\delta = 6.57$ ppm) to the PMMA methyl ester protons ($\delta = 3.59$ ppm) was found to be identical before and after hydrolysis, indicating that only the P*t*BA block and not the PMMA block

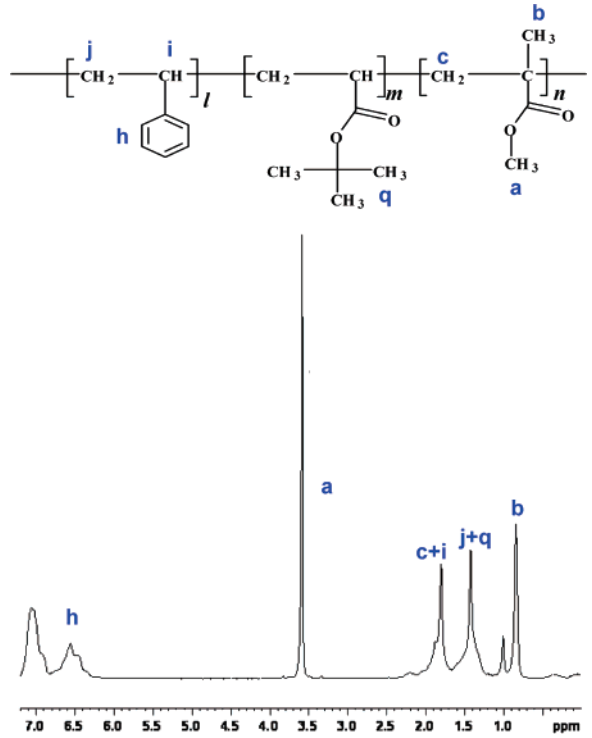

Figure 1. ^{1}H NMR spectrum and peak assignments of PS-*b*-P*t*BA-*b*-PMMA triblock copolymer in chloroform-*d*, before selective hydrolysis of the P*t*BA block.

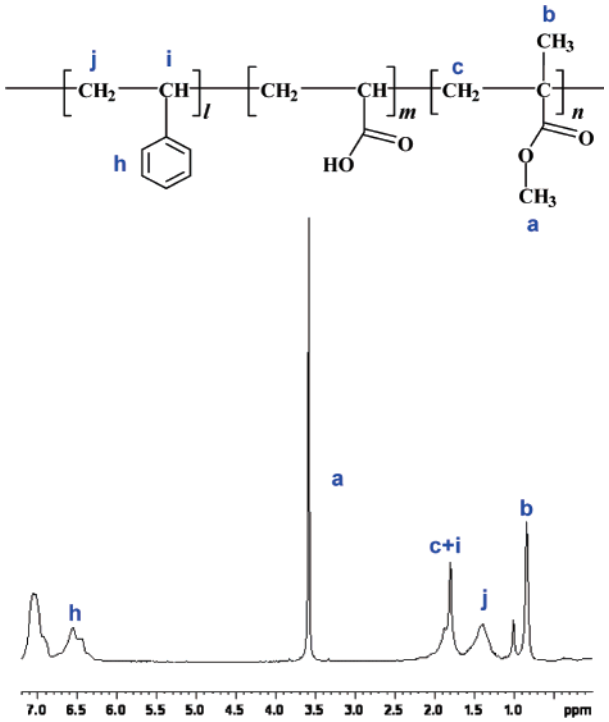

Figure 2. ^{1}H NMR spectrum and peak assignments of PS-*b*-PAA-*b*-PMMA triblock copolymer in chloroform-*d*, after selective hydrolysis of the P*t*BA block.

Table 1. Characteristics of PS-*b*-P*t*BA-*b*-PMMA Triblock Copolymer Synthesized by Sequential Anionic Polymerization

M_n, *g/mol*	M_w/M_n	N_{PS}	N_{PtBA}	N_{PMMA}
59700	1.05	296	41	236

was hydrolyzed in the reaction. Table 1 lists composition data for the hydrolyzed PS(296)-*b*-PAA(41)-*b*-PMMA(236) triblock copolymer from the combination of GPC and NMR analysis.

Copolymer Micellization and Formation of Mixed Polymer Brush-Stabilized QDs (PS/PMMA−CdS). The addition of a stoichiometric excess of cadmium acetate (1.5 mol of cadmium acetate dihydrate:1 mol of acrylic acid repeat units) to PS(296)-*b*-PAA(41)-*b*-PMMA(236) in benzene/methanol resulted in neutralization of PAA, forming a negatively charged middle block which underwent immediate self-assembly in the organic media. The appearance of a blue tinge upon addition of cadmium acetate indicated fast formation of micelles with an insoluble poly(cadmium acrylate) (PACd) core; the micellization of the triblock copolymer was confirmed by GPC following freeze-drying, washing, and resuspension of the micelles in THF (not shown). The soluble PS and PMMA end blocks form a mixed corona of PS and PMMA chains upon copolymer micellization (Scheme 1), as confirmed by later analysis. Because of the relatively long soluble PS and PMMA end blocks compared to the short middle insoluble PACd block, the resulting micelles are best described as starlike.

Exposure of freeze-dried PS-*b*-PACd-*b*-PMMA micelles to H_2S resulted in a recovered yellow powder consisting of CdS QDs encapsulated in the cores of micelles with mixed PS/PMMA coronae (Scheme 1). Subsequent reneutralization of the PAA blocks (which had been protonated during H_2S exposure) was carried out in order to stabilize the micelles, forming a high-T_g and ionically cross-linked PACd layer surrounding the QDs. We will show that these micelle-encapsulated QDs can be regarded as chemically fixed colloidal brushes, which undergo changes in conformation, but not changes in grafting density, in different solvents. The resulting QD sample coated with a mixed polymer brush of PS and PMMA chains is designated PS/PMMA−CdS.

The yellow solid PS/PMMA−CdS could be easily dispersed in organic solvents of various polarities to yield clear colloidal dispersions. Figure 3a shows photographs of the resulting dispersions in acetone, chloroform, toluene, and THF, all at a concentration of ~5 mg/mL. The clarity of the dispersions indicates good dispersion of PS/PMMA−CdS in all four solvents, including acetone, the most polar of the four solvents, which is a good solvent for PMMA but a poor solvent for PS. For comparison, Figure 3b shows dispersions in the same solvents of a sample of CdS QDs coated by a homogeneous PS brush layer (PS−CdS)[30] with PS chain length of $N_{PS} = 300$ (similar to $N_{PS} = 296$ for PS/PMMA−CdS). The PS−CdS particles are clearly well dispersed in chloroform, toluene, and THF although could not be dispersed in acetone even after 12 h sonication. The dispersion of PS/PMMA−CdS in acetone is thus attributed to the presence of PMMA chains within a mixed brush layer surrounding the QDs. This suggests a conformational rearrangement to maintain colloidal stability of PS/PMMA−CdS in solvents both "good" and "poor" for PS.

The electron-dense QDs were visualized by transmission electron microscopy (TEM) following deposition of dilute solutions of PS/PMMA−CdS onto carbon-coated TEM grids. Figure 4a shows a typical TEM image of deposited PS/PMMA−CdS, indicating a distribution of QD sizes (dark spots) formed in the cores of triblock copolymer micelles. Although the vast majority of QDs appear as individual nanoparticles on the TEM grids, larger clusters of QDs are also occasionally observed. These clusters may represent micelle clusters that form upon solvent evaporation or else larger micelle cores containing

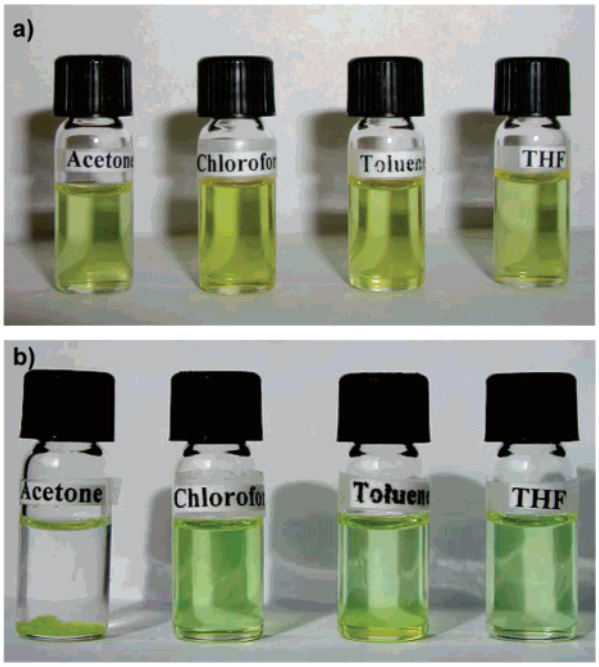

Figure 3. Photos of (a) PS/PMMA−CdS and (b) PS−CdS dispersions in acetone, chloroform, toluene, and THF.

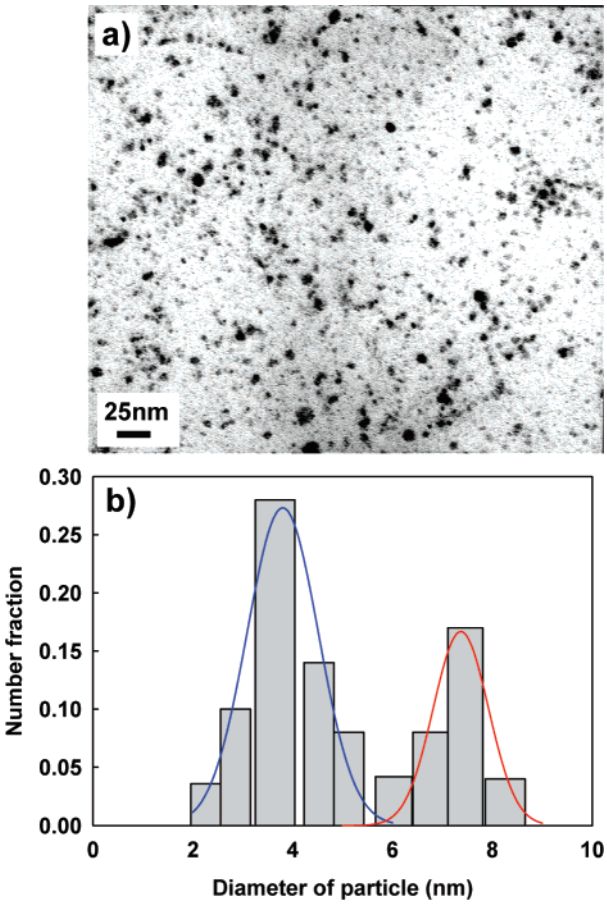

Figure 4. (a) Transmission electron micrograph (TEM) of PS/PMMA−CdS cast from a dilute (2 mg/mL) benzene dispersion onto a carbon-coated TEM grid. (b) CdS QD size distribution determined from several TEM images such as those shown in (a) taken in different regions of the grid.

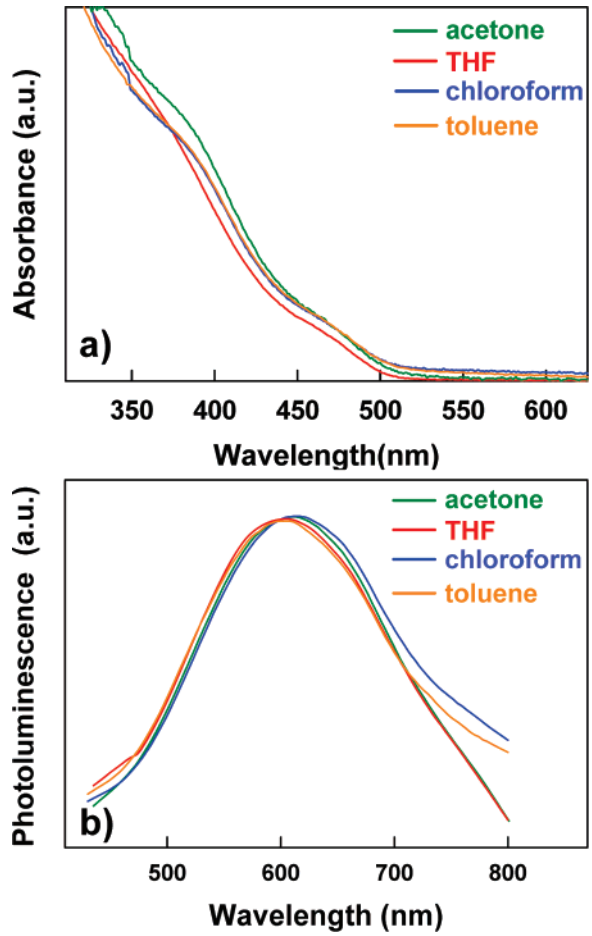

Figure 5. (a) UV−vis absorption spectra and (b) photoluminescence (PL) spectra of PS/PMMA−CdS dispersions in various solvents. For PL spectra, $\lambda_{ex} = 400$ nm.

multiple dots. Size distribution analysis (Figure 4b) was carried out based on measurement of ~300 QDs in several regions of the TEM grids, giving an average particle size and standard deviation of $2r_{CdS} = 4.9 \pm 1.8$ nm. The resulting QD diameter distribution is clearly bimodal, with a larger particle population centered at $2r_{CdS} \sim 7$ nm and a smaller particle population centered at $2r_{CdS} \sim 4$ nm. There are two possible explanations for a bimodal distribution of QDs formed in the cores of the triblock copolymer micelles: (1) the distribution of micelle aggregation numbers is itself bimodal, or (2) some micelles contain multiple very small CdS QDs due to incomplete reaction of Cd^{2+} ions in their cores, resulting in the smaller population, whereas cores in which all Cd^{2+} ions are converted into a single QD represent a significantly larger and separated QD population. CONTIN analysis of dynamic light scattering results (discussed later) show that PS/PMMA−CdS dispersed in various solvents possess a single distribution of hydrodynamic radii, which lends support to the second of the above possibilities.

Optical Properties and Stability of PS/PMMA−CdS in Various Solvents. The optical properties of PS/PMMA−CdS were determined in various solvents (acetone, THF, chloroform, toluene, in order of decreasing dielectric constant). Figure 5a shows normalized absorbance spectra of PS/PMMA−CdS dispersed in each of the four solvents. The spectra in each case are attributed to absorption of CdS QDs encapsulated in the cores of the triblock copolymer micelles. The spectra can be regarded as fingerprints of the QD size distribution via the quantum confinement effect. In each spectra, two exciton shoulders are observed at ~385 and ~470 nm, corresponding to populations of smaller and larger quantum dots, respectively, and consistent with the bimodal size distribution determined from TEM results. From the absorption threshold of the toluene solution, $\lambda_{thresh} = 512$ nm, a QD diameter of $2r_{CdS} = 7.3$ nm is determined from the following empirical formula (obtained by fitting data published previously by Henglein): $2r_{CdS} = 1/(0.1338 - 0.0002345\lambda_{thresh})$.[17,52] This size is consistent with the larger QD population ($2r_{CdS} \sim 7$ nm) determined from TEM, which is reasonable considering the higher wavelength region of the absorption spectrum corresponds to larger particles within the distribution. When the normalized spectra of PS/PMMA−CdS in different solvents are compared, they are found to overlap almost exactly (Figure 5a), indicating that the QD sizes are stable during dispersal of PS/PMMA−CdS in media of very different polarity. Normalized photoluminescence spectra of PS/PMMA−CdS in the different solvents (Figure 5b) are also similar, each showing a broad peak at ~610 nm attributed to emission from QD trap states.

Dispersions of PS/PMMA−CdS in all investigated solvents showed good long-term colloidal stability when stored in the dark under ambient conditions and remained clear without evidence of precipitation for periods of over 6 months. UV−vis absorption spectra also revealed long-term stability of QD size distributions in acetone, chloroform, and toluene (Figure 6), as evidenced by exact overlap of absorption spectra obtained on day 1 and day 180 following PS/PMMA−CdS dispersion. This indicates that the QDs are protected from agglomeration and Ostwald ripening in solvents of varying polarities ranging from acetone (dielectric constant, $\epsilon = 21$) to toluene ($\epsilon = 2.4$) within the cores of the triblock copolymer micelles. THF was the only solvent in which a noticeable change in the absorption spectrum was observed after 180 days; although the absorption threshold and exciton shoulder at 470 nm did not shift, the exciton shoulder at 385 nm disappeared over the aging period. A possible explanation is that the smaller QD population decreased due to Ostwald ripening in THF, while the maximum particle size, determined by the average number of cadmium ions in each of the original micelles, remained constant. It is not clear why THF, with an intermediate dielectric constant ($\epsilon = 7.5$), allowed for such QD ripening while the other solvents did not, although it is postulated that a combination of good solubility of both coronal blocks, along with partial swelling of the core, could explain the results.

Nuclear Overhauser Effect (NOESY) Investigation of PS/PMMA−CdS. An important question regarding the colloidal structure of PS/PMMA−CdS particles is the distribution of PS and PMMA chains in the mixed polymer brush layer. Erhardt et al. previously studied cross-linked micelles formed by self-assembly of PS-*b*-PB-*b*-PMMA triblock copolymers in the solid state, which were found to possess an asymmetric "Janus" PS/PMMA brush structure due to segregation of incompatible PS and PMMA blocks.[45,47] An important difference in the formation of PS/PMMA−CdS in the present study is that self-assembly of the PS-*b*-PAA-*b*-PMMA triblock copolymers occurred in the presence of a good solvent for both PS and PMMA, such that the dissimilar end blocks are not expected to be strongly segregated within the micelle corona; therefore, a random distribution of PS and PMMA chains around the QD cores is thought to be the most likely arrangement of the brush. 2D ^{1}H NOESY experiments probe through-space dipolar interactions of proximal protons (<0.5 nm) and were therefore employed to determine whether PS and PMMA chains were mixed or compartmentalized within PS/PMMA−CdS.[53−55]

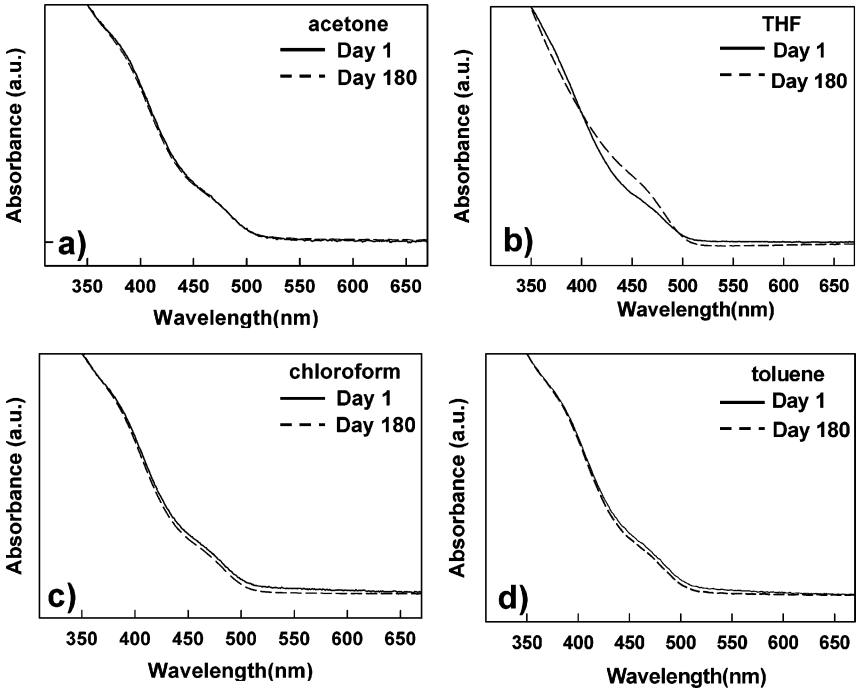

Figure 6. Investigation of long-term stability of QD size distributions for PS/PMMA−CdS dispersions in various solvents. UV−vis spectra of PS/PMMA−CdS in (a) acetone, (b) THF, (c) chloroform, and (d) toluene after 1 day (solid lines) and 180 days (dashed lines) storage under ambient conditions.

2D ^{1}H NMR NOESY spectra of PS/PMMA−CdS and the reference triblock copolymer PS(296)-*b*-PAA(41)-*b*-PMMA-(236) in THF-d_8 are shown in Figure 7. THF was chosen as the solvent since DLS experiments show that the reference triblock copolymer exists as single chains in this solvent due to the relative solubility of all three blocks, whereas PS/PMMA−CdS exists as kinetically frozen micelles. Both spectra display several off-diagonal cross-peaks, indicating proximal protons with cross-relaxation effects. In the PS/PMMA−CdS spectrum (top), distinct symmetric cross-peaks between protons of the PS and PMMA blocks are observed (red circles), specifically between phenyl ring protons on PS and methyl protons on PMMA (h, b) and between phenyl ring protons on PS and ester methyl protons on PMMA (h, a); this indicates proximal mixing of PS and PMMA segments within the brush layer. These cross-peaks are not observed in the NOESY spectrum of the reference sample (bottom), confirming that mixing between PS and PMMA blocks is a result of micelle formation and does not occur within individually solubilized chains. Significant mixing between PS and PMMA segments would not be expected if the coronal chains were compartmentalized in the manner of Janus or "patchy"[48] micelles. Thus, NOESY experiments appear to confirm the proposed random distribution of PS and PMMA chains within PS/PMMA−CdS.

Static and Dynamic Light Scattering: Solvent-Responsive Brush Conformations in PS/PMMA−CdS Colloids. Zimm plot analysis of SLS data allowed the apparent weight-average molecular weight, M_w, and the root-mean-square *z*-average radius of gyration, r_g, of the PS/PMMA−CdS particles in various solvents to be determined. Representative Zimm plots in each of the four solvents investigated are provided in the Supporting Information. Based on GPC in THF (not shown), a small fraction of unmicellized single chains (<10 wt %) is present in the PS/PMMA−CdS sample along with the micelle-encapsulated QDs; measured M_w values therefore contain a small contribution from these unmicellized chains. SLS analysis of M_w required measurement of differential refractive index values, d*n*/d*c*, for PS/PMMA−CdS in each of the solvents studied since this parameter is a component of the constant *K* within the Zimm equation (eq 1). From three repeat measurements, differential refractive index values were as follows: $dn/dc = 0.094 \pm 0.003$ (acetone); $dn/dc = 0.064 \pm 0.002$ (chloroform); $dn/dc = 0.071 \pm 0.003$ (THF); $dn/dc = 0.045 \pm 0.002$ (toluene). Using these values together with Zimm plot results, M_w values for PS/PMMA−CdS in acetone, THF, chloroform, and toluene were determined, as listed in Table 2. To calculate aggregation numbers, *Z* (Table 2), M_w values were divided by the molecular weight of a single unimer (unimer $M_{w,u} = 62\,600$ g/mol) consisting of the sum of (1) one PS(296)-*b*-PAA(41)-*b*-PMMA-(236) chain, (2) one CdS unit per carboxylate group, and (3) one Cd^{2+} ion for every two carboxylate groups. Importantly, the resulting aggregation numbers were found to be nearly identical within experimental error in all four solvents, $Z \sim 200$. This confirmed that PS/PMMA−CdS micelles are fixed by ionic cross-linking in the PACd layer, with no dynamic equilibrium between micelles and single chains in various solvents. Despite large differences in the surrounding solvent environment, therefore, the stabilizing chains are locked into the mixed polymer brush, similar to the situation of colloidal brushes with polymer chains covalently grafted to a particle surface.

The PS/PMMA−CdS aggregation number ($Z \sim 200$) allowed the chain surface density within the mixed brush layer to be estimated. Each triblock copolymer unimer in the aggregate will contribute one PS and one PMMA block, giving a total of ~400 chains within the brush; the middle block of each copolymer will contribute to the PACd layer surrounding the encapsulated QD. The PS/PMMA polymer brush is therefore grafted to a hybrid core consisting of a central QD and a surface layer of collapsed PACd chains; we estimate a total core diameter of $2r_c = 12.6$ nm based on QDs of 7.3 nm (from UV−vis) each surrounded by 200 PACd chains in the melt state. From this core size and the total number of chains, the estimated brush density is ~1.3 nm^2/chain.

Radii of gyration, r_g, of PS/PMMA−CdS particles determined from Zimm plot analysis were found to be significantly different in the various solvents, despite nearly identical aggregation

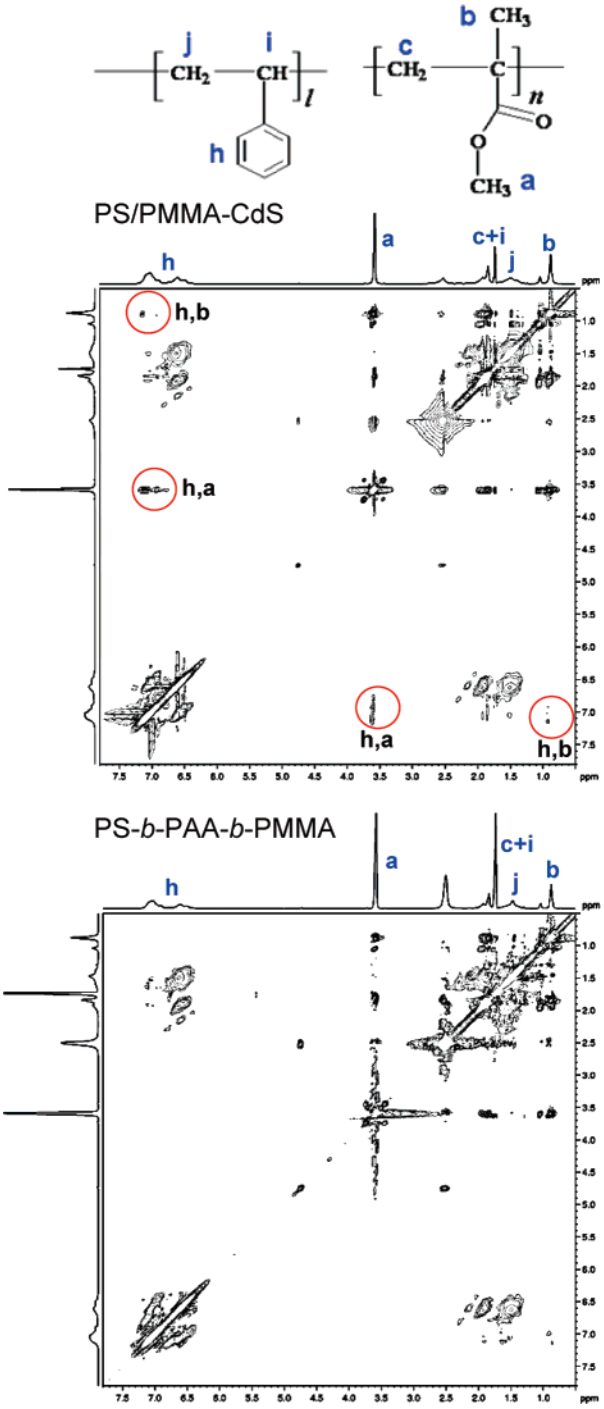

Figure 7. 2D ^{1}H NMR NOESY spectra of (a) PS/PMMA−CdS and (b) PS-*b*-PAA-*b*-PMMA in THF-d_8. Circles in (a) indicate cross-peaks between PS and PMMA blocks in the PS/PMMA−CdS spectrum which are not present in the reference spectrum (b) of PS-*b*-PAA-*b*-PMMA single chains.

numbers. These changes in r_g with constant Z provide direct evidence of conformational changes in the brush layer in response to different solvent environments. Table 2 lists r_g values for PS/PMMA−CdS in the various solvents, which range from $r_g = 24$ nm to $r_g = 41$ nm and increase in the order of r_g (acetone) < r_g (chloroform) < r_g (THF) < r_g (toluene).

PS/PMMA−CdS hydrodynamic radii, r_h, were determined from a series of multiangle and multiconcentration dynamic light scattering (DLS) experiments in each solvent. For each DLS measurement, the normalized time correlation function of the electric field was analyzed using a cumulant expansion for pointlike, isotropic particles with a distribution of particle sizes:

$$|g(\tau)| = \exp[-\bar{\Gamma}\tau + (\mu_2/2!)\tau^2 + ...] \quad (2)$$

where $\bar{\Gamma}$ is the intensity-weighted mean relaxation rate (first moment), μ_2 is the second moment, and τ is the delay time. $\bar{\Gamma}$ determined at various scattering angles is related to the effective translational diffusion coefficient D_T:

$$\bar{\Gamma} = D_T q^2 \quad (3)$$

where the scattering vector, q, depends on the refractive index of the scattering liquid, n, the wavelength of incident light, λ, and the scattering angle, θ, as follows:

$$q = \frac{4\pi n}{\lambda} \sin\left(\frac{\theta}{2}\right) \quad (4)$$

Plots of $\bar{\Gamma}$ vs q^2 obtained for each solvent and for various concentrations were found to be linear and pass through the origin in accordance with eq 3, indicating diffusive relaxation and allowing D_T to be determined from the slope. Representative plots of $\bar{\Gamma}$ vs q^2 for PS/MIC−CdS in the four solvents and at approximately the same concentration ($c \sim 0.2$ mg/mL) are shown in Figure 8a, with different slopes indicating different effective diffusion coefficients D_T in the various solvents.

To account for interparticle interactions in solution, D_T is expressed as a function of concentration:

$$D_T = D_0(1 + k_d c) \quad (5)$$

from which the single-particle diffusion coefficient, D_0, is obtained by extrapolation to zero concentration. Plots of D_T vs c for each solvent system are shown in Figure 8b. All plots are shown to be linear with small negative slopes for the THF, chloroform, and toluene systems and a larger positive slope for the acetone system; the resulting D_0 values are shown in Table 2.

The hydrodynamic radii, r_h, of PS/PMMA−CdS in the four solvents (Table 2) were calculated from D_0 values using the Stokes−Einstein equation:

$$r_h = \frac{kT}{6\pi\eta D_0} \quad (6)$$

where k is the Boltzmann constant, T is the temperature, and η is the solvent viscosity. Similar to r_g values from static light scattering, r_h values are different for each solvent, with a minimum value of $r_h = 21$ nm for acetone and a maximum value of $r_h = 31$ nm for toluene. The order of r_h values for PS/PMMA−CdS in the different solvents follows a similar trend to the r_g values, except the order of chloroform and THF are reversed: r_h(acetone) < r_h(THF) < r_h(chloroform) < r_h-(toluene). The ratio $\mu_2/\bar{\Gamma}^2$ from cumulant analysis gives a measure of particle size polydispersity in the various solvents. Similar polydispersities (0.18−0.23) were obtained in all four solvents and were consistent with polydispersity values determined previously for PS−CdS particles in toluene solutions.[20] In addition, CONTIN analysis of selected autocorrelation functions obtained at relatively low solution concentrations in each solvent (scattering angle of 90°) showed size distributions consistent with a single population of particles (Supporting Information).

Hydrodynamic radii provide a reasonable estimate for overall PS/PMMA−CdS particle sizes, including both the CdS/PACd

Table 2. Summary of PS/PMMA−CdS Structure in Various Solvents Determined from Static and Dynamic Light Scattering Data

solvent	$M_w \times 10^{-7}$, g/mol	Z	r_g, nm	$D_0 \times 10^{-7}$, nm^2 s^{-1}	r_h, nm	t_b, nm	extension, %	r_g/r_h
acetone	1.22	195	24	3.30	21	15	25 (PMMA)	1.1
THF	1.20	190	30	1.84	26	20	27 (PS)	1.2
chloroform	1.21	193	29	1.50	27	21	28 (PS)	1.1
toluene	1.31	209	41	1.26	31	25	34 (PS)	1.3

core and the solvated PS/PMMA brush layer. The difference $t_b = r_h - r_c$ gives the estimated brush thickness in each solvent (Table 2), where the core radius, $r_c = 6.3$ nm, is assumed to be constant on the basis of similar aggregation numbers in all solvents. To explain the determined r_h values in terms of PS/PMMA brush conformations, we consider literature values[56,57] of Flory−Huggins interaction parameters for each of the two chains in the four different solvents: $\chi_{PS-Ace} = 1.1$, $\chi_{PS-THF} = 0.474$, $\chi_{PS-Chl} = 0.45$, $\chi_{PS-Tol} = 0.34$, $\chi_{PMMA-Ace} = 0.18$, $\chi_{PMMA-THF} = 0.442$, $\chi_{PMMA-Chl} = 0.39$, and $\chi_{PMMA-Tol} = 0.45$.

Of the four solvents, acetone is the only poor solvent for PS ($\chi_{PS-Ace} = 1.1$), although it is an extremely good solvent for PMMA ($\chi_{PMMA-Ace} = 0.18$). PS chains within the mixed brush are therefore expected to be in a collapsed state in acetone, with the PMMA chains extended into the solvent to maintain steric stabilization of PS/PMMA−CdS (Scheme 2). In this conformation of the mixed brush, it is the end-to-end distance of the PMMA chains that will determine the overall brush thickness in acetone ($t_b = 15$ nm). The percentage extension of the PMMA chains relative to their fully stretched conformation can therefore be calculated using

$$\text{chain extension (\%)} = 100 \times (t_b/[aN]) \quad (7)$$

where $N = N_{PMMA} = 236$ and a is the length of one fully extended repeat unit ($a = 0.25$ nm). From this calculation, the chain extension of the PMMA chains in acetone is 25%. ^{1}H NMR of PS/PMMA−CdS in acetone-d_6 show distinct resonances from PS phenyl ring protons (not shown), indicating that the collapsed PS chains retain mobility due to some swelling by acetone.

The other three solvents (THF, chloroform, toluene) are good solvents for both PS and PMMA ($\chi < 0.5$), such that both types of chains will adopt extended conformations within the mixed brush layer (Scheme 2). On the basis of the interaction parameters listed above, THF and chloroform are slightly selective for PMMA while toluene is slightly selective for PS. However, despite differences in the relative stretching of PS and PMMA in these solvents, the degree of polymerization of the PS chains is significantly longer than the PMMA chains ($N_{PS} = 296 > N_{PMMA} = 236$). We therefore assume that the PS chains will extend further from the core than the PMMA chains in all three solvents and equate the brush thicknesses t_b in THF, chloroform, and toluene to the end-to-end distance of the PS chains. % PS chain extension values were calculated from eq 7 where $N = N_{PS} = 296$, giving 27% (THF), 28% (chloroform), and 34% (toluene). This order of increase in PS chain stretching within the mixed brush follows the increase in PS solvent quality, as indicated by the interaction parameters: $\chi_{PS-THF} = 0.474$, $\chi_{PS-Chl} = 0.45$, and $\chi_{PS-Tol} = 0.34$.

On the basis of the discussion above, the order of measured hydrodynamic radii (Table 2) correlates well with a simple model for solvent-responsive conformational changes within the mixed brush layer of "smart" PS/PMMA−CdS particles (Scheme 2). In acetone, the mixed brush adjusts so that the insoluble PS chains are collapsed and the soluble PMMA chains dominate the brush. On the basis of this conformation, a combination of the relatively short PMMA block length compared to PS and the decrease in steric crowding due to collapse of the PS chains (resulting in the smallest chain stretching % in acetone) explains

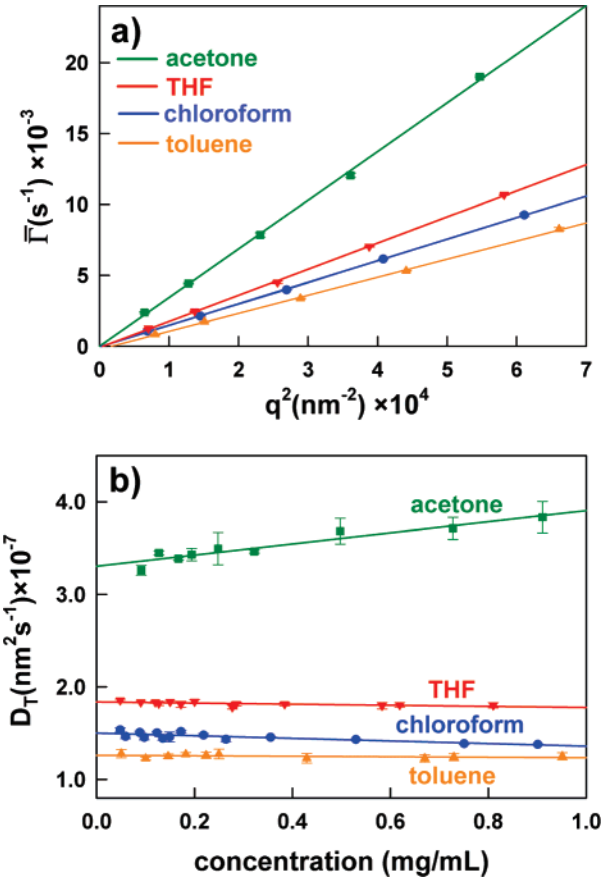

Figure 8. Dynamic light scattering (DLS) results for PS/PMMA−CdS. (a) Representative plots of $\bar{\Gamma}$ vs q^2 for PS/PMMA−CdS dispersions in different solvents of approximately equal concentration (~0.2 mg/mL). (b) Plots of D_T vs concentration for PS/PMMA−CdS in acetone, THF, chloroform, and toluene.

Scheme 2. Mixed-Brush Conformations of Environmentally Responsive PS/PMMA−CdS Nanoparticles in Different Solvents Based on DLS Data

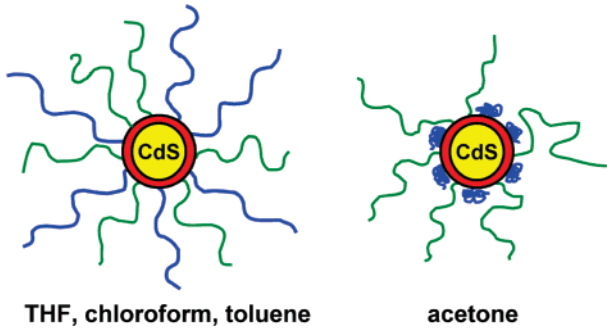

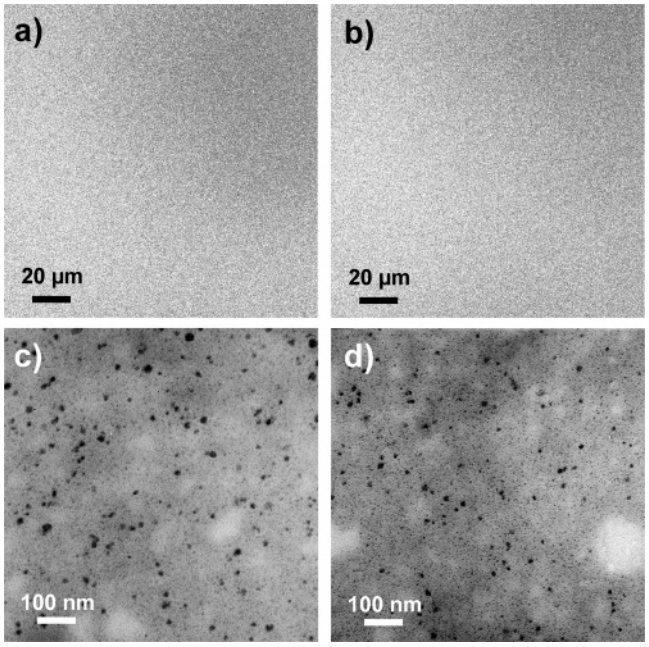

Figure 9. PS/PMMA−CdS dispersed in blend films with (a, c) PS and (b, d) PMMA homopolymer by spin-coating from toluene solutions. (a, b) Laser scanning confocal fluorescence microscopy (LSCFM) images of blend films, showing spatially uniform PL from QDs dispersed in both homopolymers. (c, d) TEM images of microtomed sections of blend films.

why r_h of PS/PMMA−CdS is smallest in acetone. In the other three solvents, both blocks are solubilized within the brush and steric crowding increases relative to acetone. With PS in an expanded state, the extension of the longer PS chains determine the brush thickness, and r_h is observed to increase in the order of increasing solvent quality for the PS block (i.e., THF < chloroform < toluene).

Further structural information is available from the ratio r_g/r_h obtained from a combination of SLS and DLS. For all solvents, ratio values are similar, in the range of 1.1−1.3, with the most expanded conformation of PS/PMMA−CdS in toluene showing the largest value of r_g/r_h (Table 2). The ratios are larger than that predicted for hard spheres, $r_g/r_h = 0.775$, but consistent with ratios reported previously for spherical starlike micelles.[58,59]

Dispersion of PS/PMMA−CdS in PS and PMMA Homopolymers. The environmentally responsive mixed brush layer also allowed PS/PMMA−CdS nanoparticles to be dispersed in both PS and PMMA homopolymers. We previously showed that PS−CdS nanoparticles can be easily dispersed in PS homopolymers due to enthalpically neutral interactions between the QD stabilizing chains and the surrounding polymer;[20,29] it has also been demonstrated that PS−CdS and PMMA homopolymer undergo fast micron-scale phase separation during spin-coating from toluene solutions due to the large positive enthalpy of mixing for PS and PMMA.[34] Here, we prepared solutions of both PS/PMMA−CdS/PS and PS/PMMA−CdS/PMMA blends in toluene and investigated the dispersion of QDs in blend films formed by spin-coating each of these solutions onto glass.

Parts a and b of Figure 9 show laser scanning confocal fluorescence microscopy (LSCFM) images of blend films of PS/PMMA−CdS nanoparticles with PS and PMMA homopolymers, respectively. The spatially homogeneous light color is due to QD PL, indicating uniform dispersion of PS/PMMA−CdS in both homopolymers on the optical length scale. PL spectra obtained for both films (Supporting Information) confirmed that the PL properties of PS/PMMA−CdS colloids were retained upon dispersion in both polymer matrices. TEM of microtomed sections indicate that the QDs were also well dispersed at the nanoscale in both PS (Figure 9c) and PMMA (Figure 9d) homopolymers. Small, light regions in the TEM images of both films (∼100 nm) are attributed to some nanoscale phase separation of the homopolymers (relatively low electron density) from the nanoparticle/homopolymer mixtures.

The observed dispersion of PS/PMMA−CdS in both PS and PMMA homopolymers by spin-coating suggests a low driving force for phase separation of the nanoparticles from either of these mutually incompatible polymers. This is attributed to the conformational response of the mixed brush during spin-coating. When the nanoparticles are blended with PS, the brush conformation will adjust to maximize surface exposure of PS segments; when the nanoparticles are blended with PMMA, the brush will maximize surface exposure of PMMA segments. In both environments, therefore, the PS/PMMA−CdS surface can adopt a conformation to minimize the positive enthalpy of mixing. However, drop-casting the same blend compositions with slow toluene evaporation over 7 days reveals significant micron-scale phase separation between PS/PMMA−CdS and both homopolymers (Supporting Information), indicating an overall unfavorable free energy of mixing between PS/PMMA−CdS and both PS and PMMA; this is attributed to a combination of entropic autophobic effects and residual surface exposure of incompatible chain segments. This shows that the demonstrated uniform dispersion of mixed-brush quantum dots in either PS or PMMA homopolymers by spin-coating is due to a combination of relatively small enthalpies of mixing and fast solvent evaporation.

Conclusions

We have prepared the first example of semiconductor quantum dots (QDs) with a mixed PS/PMMA stabilizing brush layer (PS/PMMA−CdS) via the self-assembly of a PS-*b*-PAA-*b*-PMMA triblock copolymer followed by templated growth of cadmium sulfide QDs in the ionic micelle cores. These QDs can be dispersed in solvents with wide-ranging polarities, including acetone, which is a nonsolvent for the PS chains. UV−vis and photoluminescence data demonstrate that QD sizes and optical properties are independent of the solvent medium, with demonstrated long-term stability in most solvents. 2D ^{1}H NOESY experiments on PS/PMMA−CdS in THF indicate intimate mixing of PS and PMMA segments, confirming that PS and PMMA chains are statistically distributed within the mixed brush layer. Static light scattering (SLS) of PS/PMMA−CdS indicate that particle molecular weights are nearly identical in the various solvents, showing that the copolymer chains are locked into the mixed brush via kinetic freezing of the poly(cadmium acrylate) layer. A combination of SLS and dynamic light scattering (DLS) shows significant changes in r_g and r_h for PS/PMMA−CdS in the various solvents, with r_h values increasing in the order acetone < THF < chloroform < toluene. Changes in hydrodynamic particle size are explained by solvent-responsive conformational changes in the mixed brush layer in order to maintain colloidal stability in different solvent media. In addition, conformational changes in the mixed brush allow PS/PMMA−CdS QDs to be well dispersed in both PS and PMMA homopolymers. Studies on the application of these QDs with mixed polymer brush layers for three-dimensional self-assembly in colloids and polymer blends are currently underway in our laboratory.

Acknowledgment. The authors gratefully acknowledge the Natural Science and Engineering Research Council of Canada

(NSERC), the Canadian Foundation for Innovation (CFI), and the British Columbia Knowledge Development Fund (BCKDF) for their support of the research.

Supporting Information Available: Gel permeation chromatograms for each step of anionic polymerization of PS-*b*-P*t*BA-*b*-PMMA; representative Zimm plots of PS/PMMA−CdS in various solvents; CONTIN size distributions of PS/PMMA−CdS in various solvents; photoluminescence spectra of PS/PMMA−CdS dispersed in PS and PMMA homopolymers; laser scanning confocal microscopy images of blend films of PS/PMMA−CdS and both PS and PMMA homopolymers, drop-cast from toluene with slow solvent evaporation. This material is available free of charge via the Internet at http://pubs.acs.org.

References and Notes

(1) von Werne, T.; Patten, T. E. *J. Am. Chem. Soc.* **1999**, *121*, 7409.
(2) Farmer, S. C.; Patten, T. E. *Chem. Mater.* **2001**, *13*, 3920.
(3) Carrot, G.; Rutot-Houze, D.; Pottier, A.; Degee, P.; Hilborn, J.; Dubois, P. *Macromolecules* **2002**, *35*, 8400.
(4) Ohno, K.; Koh, K.; Tsujii, Y.; Fukuda, T. *Macromolecules* **2002**, *35*, 8989.
(5) Skaff, H.; Ilker, M. F.; Coughlin, E. B.; Emrick, T. *J. Am. Chem. Soc.* **2002**, *124*, 5729.
(6) Sill, K.; Emrick, T. *Chem. Mater.* **2004**, *16*, 1240.
(7) Carrot, G.; Scholz, S. M.; Plummer, C. J. G.; Hilborn, J. G. *Chem. Mater.* **1999**, *11*, 3571.
(8) Corbierre, M. K.; Cameron, N. S.; Sutton, M.; Mochrie, S. G. J.; Lurio, L. B.; Ruhm, A.; Lennox, R. B. *J. Am. Chem. Soc.* **2001**, *123*, 10411.
(9) Potapova, I.; Mruk, R.; Prehl, S.; Zentel, R.; Basche, T.; Mews, A. *J. Am. Chem. Soc.* **2003**, *125*, 320.
(10) Skaff, H.; Emrick, T. *Chem. Commun.* **2003**, 52.
(11) Tadd, E.; Zeno, A.; Zubris, M.; Dan, N.; Tannenbaum, R. *Macromolecules* **2003**, *36*, 6497.
(12) Wang, X.-S.; Dykstra, T. E.; Salvador, M. R.; Manners, I.; Scholes, G.; Winnik, M. A. *J. Am. Chem. Soc.* **2004**, *126*, 7784.
(13) Corbierre, M. K.; Cameron, N. S.; Sutton, M.; Laaziri, K.; Lennox, R. B. *Langmuir* **2005**, *21*, 6063.
(14) Wang, M.; Oh, J. K.; Dykstra, T. E.; Lou, X.; Scholes, G. D.; Winnik, M. A. *Macromolecules* **2006**, *39*, 3664.
(15) Moller, M.; Kunstle, H.; Kunz, M. *Synth. Met.* **1991**, *41*−*43*, 1159.
(16) Cummins, C. C.; Schrock, R. R.; Cohen, R. E. *Chem. Mater.* **1992**, *4*, 27.
(17) Moffitt, M.; McMahon, L.; Pessel, V.; Eisenberg, A. *Chem. Mater.* **1995**, *7*, 1185.
(18) Forster, S.; Antonietti, M. *Adv. Mater.* **1998**, *10*, 195.
(19) Spatz, J. P.; Herzog, T.; Mossmer, S.; Ziemann, P.; Moller, M. *Adv. Mater.* **1999**, *11*, 149.
(20) Wang, C.-W.; Moffitt, M. G. *Langmuir* **2004**, *20*, 11784.
(21) Zhang, M.; Drechsler, M.; Muller, A. H. E. *Cherm. Mater.* **2004**, *16*, 537.
(22) Bennett, R. D.; Miller, A. C.; Kohen, N. T.; Hammond, P. T.; Irvine, D. J.; Cohen, R. E. *Macromolecules* **2005**, *38*, 10728.
(23) Kang, Y.; Taton, T. A. *J. Am. Chem. Soc.* **2003**, *125*, 5650.
(24) Kang, Y.; Taton, T. A. *Angew. Chem., Int. Ed.* **2005**, *44*, 409.
(25) Kang, Y.; Taton, T. A. *Macromolecules* **2005**, *38*, 6115.
(26) Filali, M.; Meier, M. A. R.; Schubert, U. S.; Gohy, J.-F. *Langmuir* **2005**, *21*, 7995.
(27) Duxin, N.; Liu, F.; Vali, H.; Eisenberg, A. *J. Am. Chem. Soc.* **2005**, *127*, 10063.
(28) Niu, H.; Zhang, L.; Gao, M.; Chen, Y. *Langmuir* **2005**, *21*, 4205.
(29) Wang, C.-W.; Moffitt, M. G. *Langmuir* **2005**, *21*, 2465.
(30) Yusuf, H.; Kim, W.-G.; Lee, D.-H.; Guo, Y.; Moffitt, M. G. *Langmuir* **2007**, *23*, 868.
(31) Yusuf, H.; Kim, W.-G.; Lee, D.-H.; Aloshyna, M.; Brolo, A. G.; Moffitt, M. G. *Langmuir*, in press.
(32) Cheyne, R. B.; Moffitt, M. G. *Langmuir* **2005**, *21*, 10297.
(33) Cheyne, R. B.; Moffitt, M. G. *Macromolecules* **2007**, *40*, 2046.
(34) Wang, C.-W.; Moffitt, M. *Chem. Mater.* **2005**, *17*, 3871.
(35) Zhang, Z.; Horsch, M. A.; Lamm, M. H.; Glotzer, S. C. *Nano Lett.* **2003**, *3*, 1341.
(36) Zhang, Z.; Glotzer, S. C. *Nano Lett.* **2004**, *4*, 1407.
(37) Zhang, Z.; Keys, A. S.; Chen, T.; Glotzer, S. C. *Langmuir* **2005**, *21*, 11547.
(38) Vanakaras, A. G. *Langmuir* **2006**, *22*, 88.
(39) Li, D.; Sheng, X.; Zhao, B. *J. Am. Chem. Soc.* **2005**, *127*, 6248.
(40) Shan, J.; Nuopponen, M.; Jiang, H.; Viitala, T.; Kauppinen, E.; Kontturi, K.; Tenhu, H. *Macromolecules* **2005**, *38*, 2918.
(41) Shan, J.; Chen, J.; Nuopponen, M.; Viitala, T.; Jiang, H.; Peltonen, J.; Kauppinen, E.; Tenhu, H. *Langmuir* **2006**, *22*, 794.
(42) Chiu, J. J.; Kim, B. J.; Kramer, E. J.; Pine, D. J. *J. Am. Chem. Soc.* **2005**, *127*, 5036.
(43) Zubarev, E. R.; Xu, J.; Sayyad, A.; Gibson, J. D. *J. Am. Chem. Soc.* **2006**, *128*, 4958.
(44) Zubarev, E. R.; Xu, J.; Sayyad, A.; Gibson, J. D. *J. Am. Chem. Soc.* **2006**, *128*, 15098.
(45) Erhardt, R.; Boker, A.; Zettl, H.; Kaya, H.; Pyckhout-Hintzen, W.; Krausch, G.; Abetz, V.; Muller, A. H. E. *Macromolecules* **2001**, *34*, 1069.
(46) Xu, H.; Erhardt, R.; Abetz, V.; Muller, A. H. E.; Goedel, W. A. *Langmuir* **2001**, *17*, 6787.
(47) Erhardt, R.; Zhang, M.; Boker, A.; Zettl, H.; Abetz, C.; Frederik, P.; Krausch, G.; Abetz, V.; Muller, A. H. E. *J. Am. Chem. Soc.* **2003**, *125*, 3260.
(48) Hoppenbrouwers, E.; Li, Z.; Liu, G. *Macromolecules* **2003**, *36*, 876.
(49) Hautekeer, J.-P.; Varshney, S. K.; Fayt, R.; Jacobs, C.; Jerome, R.; Teyssie, P. *Macromolecules* **1990**, *23*, 3893.
(50) Zhong, X. F.; Varshney, S. K.; Eisenberg, A. *Macromolecules* **1992**, *25*, 7160.
(51) Guegan, P.; Cernohous, J. J.; Khandpur, A. K.; Hoye, T. R.; Macosko, C. W. *Macromolecules* **1996**, *29*, 4605.
(52) Henglein, A. *Chem. Rev.* **1989**, *89*, 1861.
(53) Cammas, S.; Harada, A.; Nagasaki, Y.; Kataoka, K. *Macromolecules* **1996**, *29*, 3227.
(54) Vangeyte, P.; Leyh, B.; Auvray, L.; Grandjean, J.; Misselyn-Baudin, A.-M.; Jerome, R. *Langmuir* **2004**, *20*, 9019.
(55) Voets, I. K.; de Keizer, A.; Cohen Stuart, M. A.; de Waard, P. *Macromolecules* **2006**, *39*, 5952.
(56) Xuan, Y.; Peng, J.; Cui, L.; Wang, H.; Li, B.; Han, Y. *Macromolecules* **2004**, *37*, 7301.
(57) Shiomi, T.; Kuroki, K.; Kobayashi, A.; Nikaido, H.; Yokoyama, M.; Tezuka, Y.; Imai, K. *Polymer* **1995**, *36*, 2443.
(58) Forster, S.; Zisenis, M.; Wenz, E.; Antonietti, M. *J. Chem. Phys.* **1996**, *24*, 9956.
(59) Moffitt, M.; Eisenberg, A. *Macromolecules* **1997**, *30*, 4363.

MA070855X